PROCEEDINGS OF SPIE

SPIEDigitalLibrary.org/conference-proceedings-of-spie

Long-distance entanglement distribution through satellite intermediary entanglement swapping

John Floyd, Paul Kwiat

John Floyd, Paul Kwiat, "Long-distance entanglement distribution through satellite intermediary entanglement swapping," Proc. SPIE 12446, Quantum Computing, Communication, and Simulation III, 124460L (8 March 2023); doi: 10.1117/12.2650193

SPIE.

Event: SPIE Quantum West, 2023, San Francisco, California, United States

Long-distance entanglement distribution through satellite intermediary entanglement swapping

John Floyd[a] and Paul Kwiat[a]

[a]University of Illinois Urbana-Champaign, 1110 W Green St Loomis Laboratory, Urbana, IL 61801

ABSTRACT

Efficient transcontinental entanglement distribution is necessary to build a global quantum network. Without quantum repeaters, distribution through optical fibers is assailed by loss and scattering, limiting the network's reach to around 100 kilometers. This distance can be greatly extended however, by transmitting photons through free space, where the transmission falls only as the reciprocal square of the propagation distance. Our experiment aims to prove the viability of one proposed satellite intermediary scheme: a down-link architecture using entanglement swapping. In this scheme, a satellite generates a pair of entangled photons that are spectrally unentangled – and therefore able to interfere with other photons. The satellite transmits the telecom pump and the entangled telecom photons down to a station on Earth's surface; by doing so, both channels experience the same temporal drift due to Doppler shift and dispersion. The transmitted pump can then be collected, reamplified, and used to pump a second terrestrial entanglement source. Synchronizing and interfering the satellite and terrestrial entangled, telecom photons will then swap entanglement to the unused photons. We are implementing this by pumping non-degenerate entanglement sources, which produce daughter photons at 773 nm and 1588 nm, with a 520 nm pump, generated from third harmonic generation.

Keywords: Quantum communication, Entanglement, Entanglement distribution, Swapping

INTRODUCTION

Proposed quantum technologies and communication schemes have the potential to revolutionize scientific research and stimulate economic growth. Promising results are beginning to manifest, such as the 2019 milestone proof of quantum supremacy by Google's quantum computer,[1] detection of gravitational waves using high-precision quantum sensing techniques,[2] breakthroughs toward the quantum internet,[3] and other future applications in disease research,[4] machine learning,[5] communication,[6] high-precision sensing,[7] and security.[8] The pursuit of a global quantum network is an important next step.

In classical channels, a device called an optical repeater can amplify signals for long-distance communication. However, due to the No-Cloning Theorem of quantum mechanics,[9] if the same technique is performed on a quantum channel, the amplification introduces too much noise, necessarily resulting in reduced quantum state fidelity. Research is on going to produce quantum repeaters, the quantum analog of optical repeaters, which can revitalize entangled qubits over long distances.[10] However, quantum repeaters are in the early stages of development, and subsequently, a high efficiency, scalable quantum repeater is still likely years away.

So far, quantum entanglement, encoded in photons, has been shown to be preserved at distances up to around 100 km in both free-space[11] and fiber-optic links[12] on Earth's surface. Due to exponential attenuation in optical fiber per unit length, typically 0.2 dB/km, links beyond ∼200 km are untenable. In contrast, free-space channels can preserve entanglement better and with higher rates. In 2017, successful satellite-to-ground entanglement distribution was performed between ground stations up to 2400 km apart.[13] In this experiment, entanglement from a spontaneous parametric down-conversion (SPDC) source stationed on a satellite at an altitude of ∼500 km was distributed to two stations on Earth's surface. Entanglement was then verified by performing a Bell's inequality violation.[14] While this demonstration shows the viability of satellite-enhanced entanglement distribution, the source utilized produced distinguishable photons, which cannot be used for more general protocols like teleportation.

Quantum Computing, Communication, and Simulation III, edited by Philip R. Hemmer, Alan L. Migdall, Proc. of SPIE Vol. 12446, 124460L · © 2023 SPIE · 0277-786X · doi: 10.1117/12.2650193

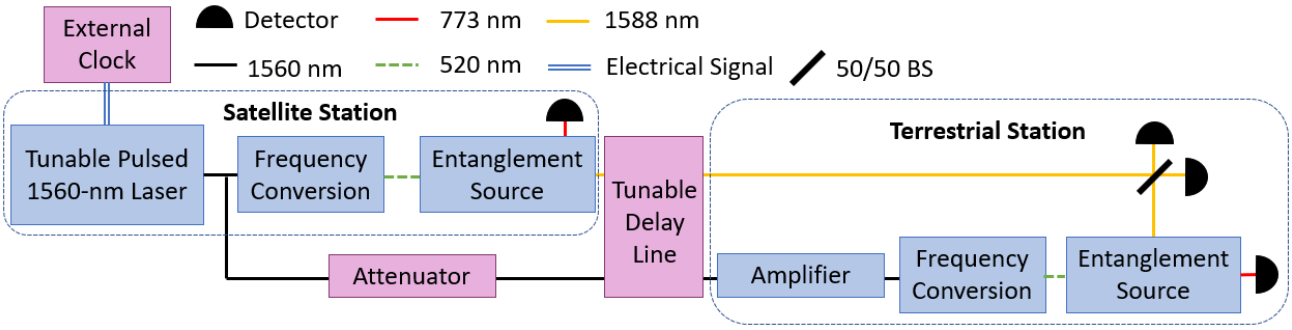

Figure 1. General experimental apparatus. Blue boxes represent components that are necessary for the down-link architecture. Pink boxes represent components that simulate real-world phenomena and would be likely excluded when this scheme is performed in practice. The 50/50 beamsplitter is used as a Bell state analyzer for entanglement swapping.

Entanglement swapping can be used to connect two separate entangled sources by interfering one photon from each source and swapping entanglement to the other photons, which have never interacted. This is the primary phenomenon for repeaters in a quantum network. When combined with quantum memories, this would allow transmission up to to any arbitrary distance, limited by the number of available entanglement sources. Entanglement swapping has been demonstrated over 100 km of optical fiber,[15] with multiparticle states,[16] and with 3 different entanglement sources.[17] However, no current demonstration of entanglement swapping has been performed between relatively moving platforms, a milestone necessary for satellite demonstrations.

High visibility interference between sources requires the photons be indistinguishable and therefore precisely synchronized. Specifically, the photons from the two sources must arrive at the final beamsplitter simultaneously to within their reciprocal bandwidth; in typical SPDC experiments this corresponds to synchronization arrival time differences less than a picosecond. This is obviously very challenging when one or both of the sources is moving rapidly with respect to the beamsplitter. We address this synchronization problem by using a down-link architecture where a shared pump laser on a satellite pumps both a source in space and a source on the ground. Under this scheme, photon pairs generated from both sources should experience the same Doppler shift, atmospheric turbulence, and path length changes due to positional jitter.

METHODS & EQUIPMENT

Sources & Laser

Our experimental apparatus is shown in Fig. 1.

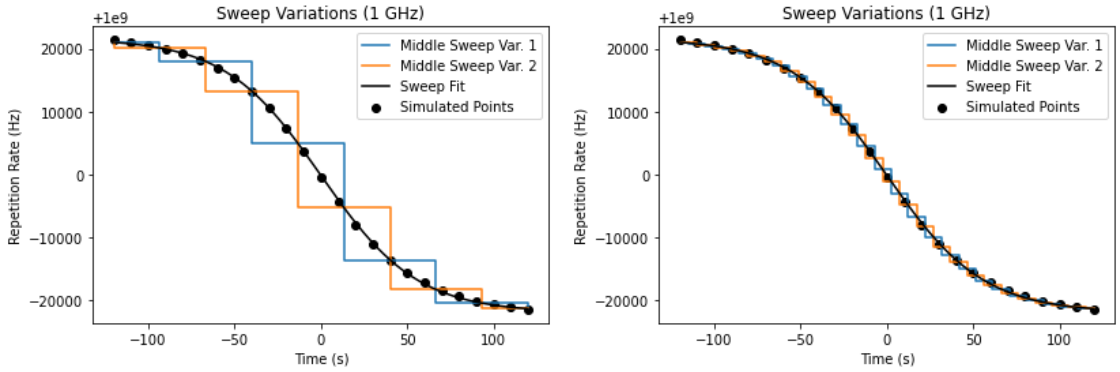

Figure 2. Fits to simulate Doppler shift. The International Space Station's orbital velocities were used to calculate the expected laser repetition rate Doppler shift. Our signal generator could model this shift by performing list sweeps, using upwards of 10000 data values. **LEFT:** 10 data points ; **RIGHT:** 100 data points.

We generate 773-nm and 1588-nm single photons through spontaneous parametric down-conversion (SPDC) in type-II, periodically poled potassium titanyl phosphate (ppKTP) crystals. By pumping the ppKTP crystal in two different spatial modes and recombining, we can produce a bipartite polarization-entangled state, Fig. 3. Our ppKTP crystal length, 20 mm, was chosen to narrow the daughter photon's bandwidth, increasing its pulsewidth, and easing source synchronization. In addition, an etalon with a 0.45-nm FWHM bandwidth is placed in the 1588-nm daughter photon path to further broaden the pulsewidth and remove spectral entanglement between the daughter photons. If the source were to remain spectrally entangled, we would be able to distinguish between the interfering photons by measuring the spectrum of their sister photons, which would be detrimental to the interference necessary to perform entanglement swapping. To verify this loss in spectral entanglement, we performed a $g^2(\tau = 0)$ auto-correlation measurement on the 1588-nm path using a Hanbury-Brown-Twiss (HBT) configuration.[18]

Our 520-nm entanglement source pump is produced through frequency conversion of a amplified, via an erbium-doped fiber amplifier (EDFA) made by PriTel Inc., and pulsed 1560-nm signal using third harmonic generation (THG). The repetition rate of the laser was set to 1.155 GHz to stifle self-phase modulation (SPM) in the optical fiber before our frequency conversion setup. SPM is a nonlinear process that can change the bandwidth of a laser. This phenomenon increases with the laser's peak power and the length of the fiber. We therefore increased the repetition rate of the laser while keeping the average power the same so as to reduce the peak power. This change in bandwidth negatively impacted our resultant THG efficiency.

Our laser repetition rate can be locked to an external signal. A feedback loop maintains mode-locking through small shifts in the external signal's repetition rate. This is utilized to simulate the expected Doppler shift in the repetition rate between a signal sent from a satellite in low-earth orbit to a ground station on Earth's surface, Fig. 2. Because the expected motional Doppler shift in the frequency of the light (4 GHz) is much smaller than our photon's bandwidth (53.5 GHz, assuming 0.45-nm bandwidth), this shift should not significantly impact our final results.

Simulation Components

To verify the real-world applicability of our apparatus, we have designed and are in the process of implementing experimental components to simulate random jitters, attenuation, and motional-induced Doppler shift on the

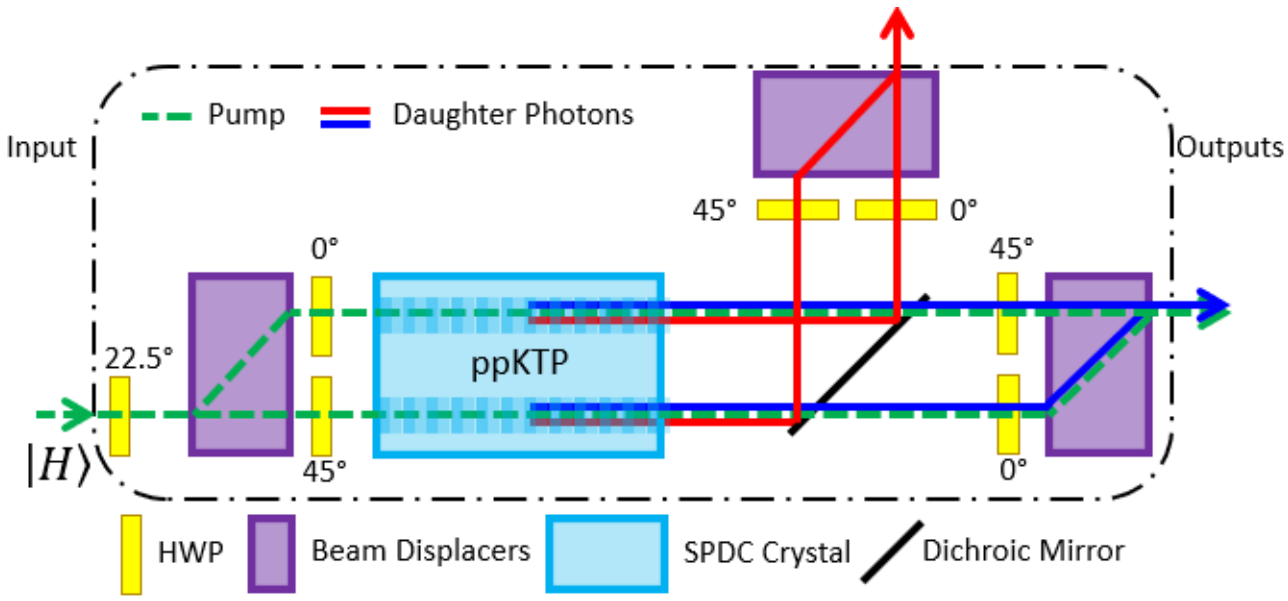

Figure 3. A beam displacer source, shown above, is utilized to generate a bipartite, polarization-entangled state by pumping a down-conversion crystal in two spatial modes. The half-wave plates (HWP) alter each path's polarization to recombine the paths using a second beam displacer downstream. The pump's central wavelength is 520-nm and has a 0.2-nm bandwidth. The source is nondegenerate and produces daughter photons at 1588 nm and 773 nm.

laser repetition rate. Since the wavelengths of our pump (1560-nm) and transmitted telecom single photons (1588-nm) are quite close, atmospheric dispersion impacts our expected interference visibility by less than 1%. There are plans to simulate dispersion in our tunable delay line; however, its priority is lower than other synchronization issues.

As described above, we simulate the motionally induced Doppler shift is simulated by varying an external (digital) signal generator's output frequency. The generator was initially purchased for ease of use and for its low phase noise; however, it was later found that the time period between data values - the switching speed - is slow enough (30 μs) to often cause our pulsed laser to lose mode-locking. For the measurements described here, we post-select on the cases where the laser remains mode-locked over the Doppler shift sweep; in the future, we are looking into analog equivalents such as using voltage-controlled oscillators (VCO). Note that in the actual final application, we will not need to vary the laser frequency, here it is done simply to simulate the Dopper shift between moving platforms.

Our 1560-nm laser is split into 2 different spatial modes. One spatial mode travels to our satellite station's frequency conversion setup and entanglement source. The other is attenuated to mimic propagation from space to earth before being re-amplified by a second EDFA. Due to SPM on the output of this second amplifier, we utilize a free-space, spatial attenuation technique, involving a knife-edge; otherwise, the pulsewidth was found to change and cause poor THG efficiency at the terrestrial station.

In addition to the deterministic motional Doppler shift, path length jitter is simulated through our tunable delay line, Fig. 1. Both the 1588-nm photons from our satellite station and the attenuated pulsed laser signal travel through this delay line in the same spatial mode. The delay line consists of three retro-reflectors oriented so that the light reflects back through the system but displaced by 1-inch. One retro-reflector is placed on top of a 0.6-meter long, motorized translation stage. With 3 retro-reflectors, this gives us 2.4 meters of overall delay. The translation stage will be configured to simulate jitter or consistent distance changes by traveling through a predefined path during a measurement.

Bell State Analyzer & Detectors

Our Bell state analyzer consists of a 50/50 beam-splitter (BS) and 2 differential-readout superconducting nanowire single-photon detectors (SNSPDs). As long as the 1588-nm photons from both entanglement sources are indistinguishable on our 50/50 BS, they should experience interference through the Hong-Ou-Mandel (HOM) effect. Through the HOM effect, we can distinguish the $|\Psi^-\rangle = \frac{1}{\sqrt{2}}(|HV\rangle - |VH\rangle)$ Bell state from the others when we register a coincidence between the two detectors after our 50/50 BS, shown in Fig. 1. In order to exclude events where both photons after the BS come from the same source, we instead look for 4-fold coincidences on

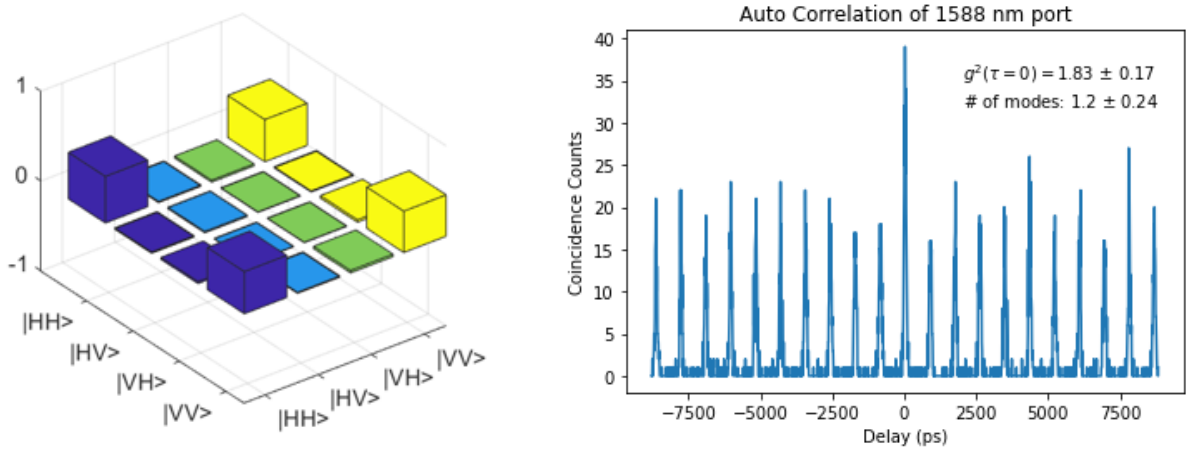

Figure 4. **LEFT:** State tomography results of one of our entanglement sources. The plot shows the values for the density matrix representation of the expected $|\Psi^+\rangle$ state. **RIGHT:** Plot of our $g^2(\tau = 0)$ auto-correlation HBT measurement. This data set was taken over 4 hours.

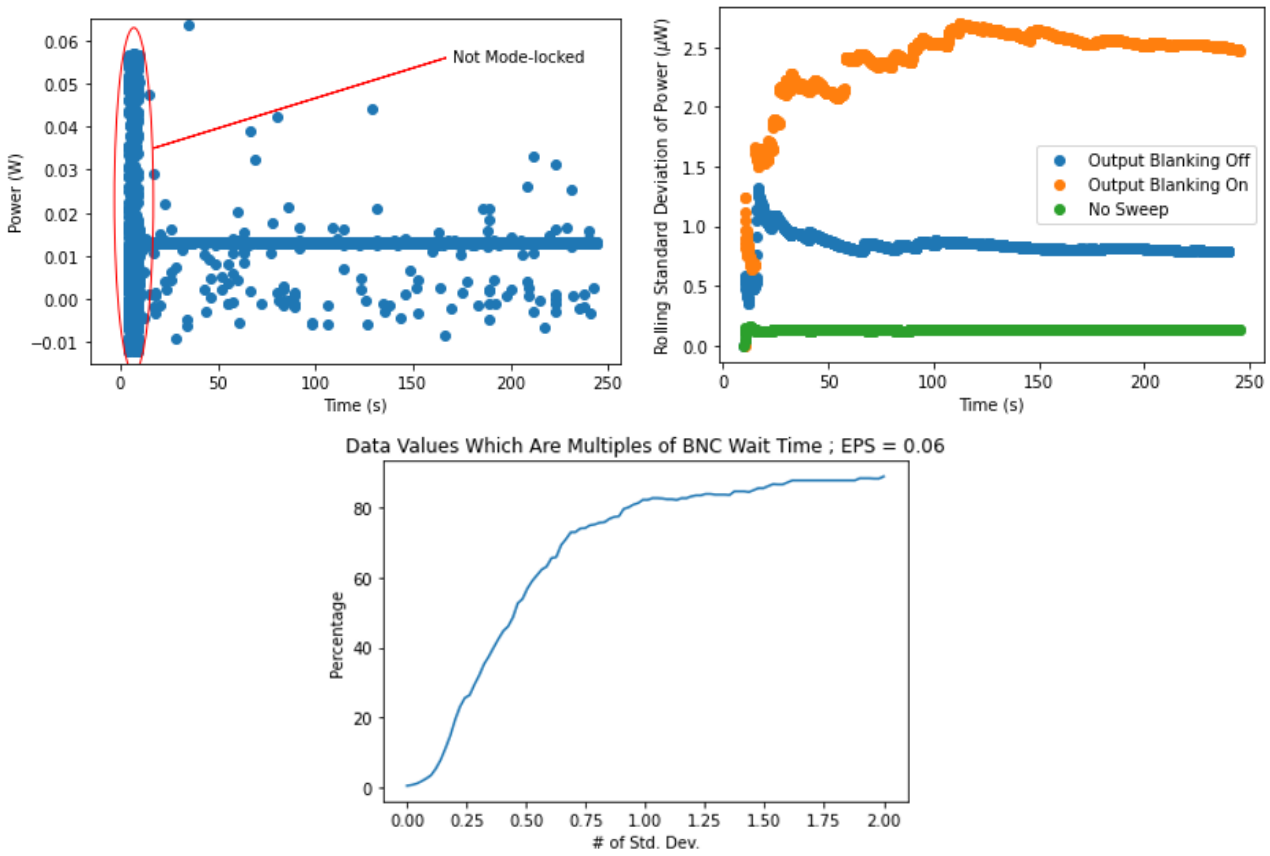

Figure 5. **TOP LEFT:** Average power measurement over a repetition rate sweep. The blue vertical bar at the beginning is a series of quick oscillations in power caused by our laser losing mode-locking. **TOP RIGHT:** Plot of the standard deviation of laser power over the sweep for several cases: 1) no sweep, 2) sweep where external signal turns off between data values (Output Blanking ON), and 3) sweep where external signal remains on between data values (Output Blanking OFF). There is enough drift with Output Blanking OFF to still require post-selection. **BOTTOM:** Proof that points of high standard deviation occur at multiples of the signal generator's time between switching. As we look further from the mean power, the data points become multiples of time between switching. This indicates that the outlier points are due to

all four detectors. Selecting these cases ensures we only include counts that originated from events where each source generated an entangled pair of photons.

PRELIMINARY RESULTS & DISCUSSION

Sources & Laser

Our entanglement sources meet necessary swapping requirements, but their overall count rates are lower than expected. We can obtain quantum states with fidelities of 96%, with the expected $|\Psi^+\rangle = \frac{1}{\sqrt{2}}(|HH\rangle + |VV\rangle)$ Bell state from our entanglement sources. A typical quantum state tomography output is shown in Fig. 4. Furthermore, we measured a $g^2(\tau = 0) = 1.83 \pm 0.17$ using an auto-correlation HBT measurement on the 1588-nm output port with the etalon in place. This corresponds to around 1.2 spectral modes, indicating a swappable source. We collected statistics for our $g^2(\tau = 0)$ measurement over a 4 hours. Our sources are capable to producing 20-25k cps 773-nm and 1588-nm singles and 4-5k cps coincidences; the coincidences drop to 300-500 cps when our etalon is placed in the 1588-nm path. With this information, we can approximate the average photon number to be around 10^{-4} using 12 mW of average pump power, so that double pair events are negligible.

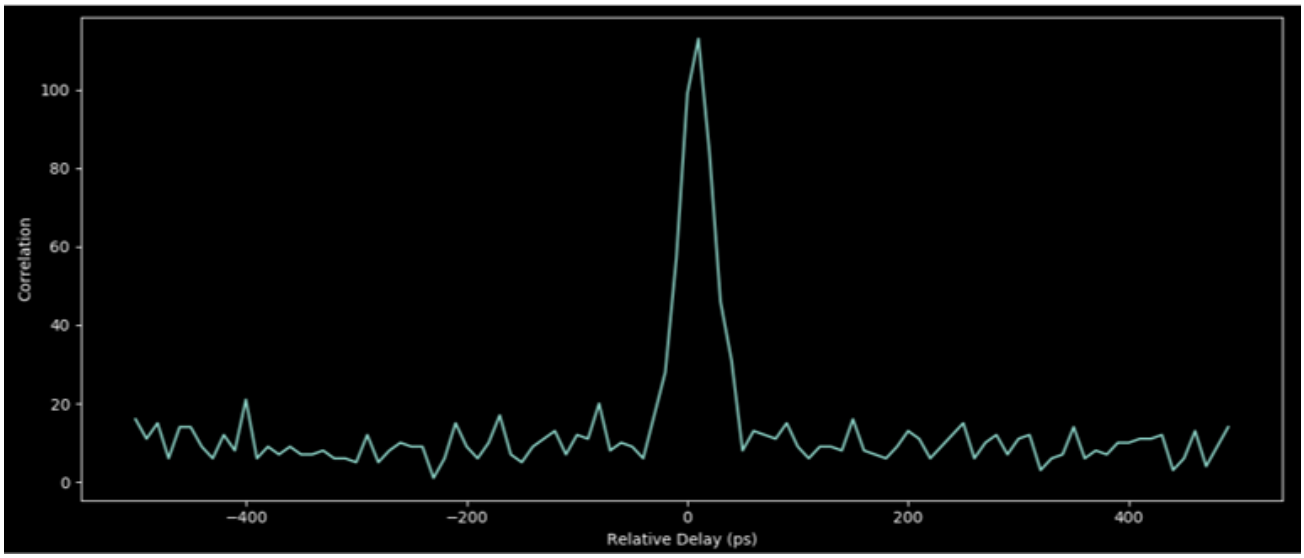

Figure 6. Example plot of our coincidence counts with etalon in place. Output gives us an understanding of the jitter, timing resolution, of our system and detectors. Measured FWHM jitter: 30 ps.

While having high count rates is not necessary to show swappability over moving platforms, it allows us to perform measurements quicker. We are pursuing increasing our source rates by minimizing SPM and optimizing the frequency conversion system, i.e. matching the beam waist and improving coupling efficiency.

Simulation Components

Our laser remains mode-locked through most of the external signal generator's sweep; the shape of the sweep is shown in Figure 2. We verified the laser's continual mode-locking through a heuristic test that measured the laser's output power during the sweep, Fig. 5. This technique was employed since the change in laser repetition rate was below the resolution of our photodiodes and oscilloscopes. Instead, we monitored the average output power of the laser, which produces quick power fluctuations when it is not mode-locked. The fluctuations near the beginning of the plot indicate when the laser was not mode-locked, i.e., the laser power drifts several standard deviations away from the expected mean. Based on our power-meter data, this period of time is on the order of magnitude of several milliseconds. When measuring entanglement swapping over a sweep, we can post-select on the cases where we do not observe a jump in the average output power.

The components for the tunable delay line, observe Fig. 1, have recently been purchased and are almost all received. In the future, we will perform swaps between the entanglement sources after a varying delay is applied.

Bell State Analyzer & Detectors

Our Bell state analyzer (BSA) is built, and several hundred 1588-nm singles counts per second from each source have been measured traveling through the system. We are currently working to improve the source brightness and coupling to the BSA.

Our SNSPD detectors, with center wavelengths at 1588 nm and 800 nm, have been installed and are working well. A plot of a SNSPD timing jitter can be seen in Figure 6.

CONCLUSION

We have reached several important milestones to show the viability of entanglement swapping between fast moving platforms. Our entanglement sources produce high state quality and minimal spectral entanglement. Furthermore, sweeping our laser's repetition rate via an external signal generator has produced promising results. The next immediate step is to measure Hong-Ou-Mandel interference between both sources. However, while our Bell state analyzer is built and our detectors are operational, we are currently limited by our sources' low count rates.

ACKNOWLEDGEMENTS

This work was funded by NASA grant 80NSSC20K0629. Special thanks to Joseph Chapman, now a postdoctoral research associate at ORNL, for jump-starting this project and mentoring me in my first year of graduate school. Also, thank you to K V Reddy at PriTel and Boris Kurzh at JPL for lending helping hands when instruments did not work as intended and being patient when I just thought they didn't.

REFERENCES

[1] Arute, F., Arya, K., and Babbush, R. e. a., "Quantum supremacy using a programmable superconducting processor.," *Nature* **574**, 505–510 (2019).

[2] Aasi, J., Abadie, J., and Abbott, B. e. a., "Enhanced sensitivity of the ligo gravitational wave detector by using squeezed states of light.," *Nature Photonics* **7**, 613–619 (2013).

[3] Wehner, S., Elkouss, D., and Hanson, R., "Quantum internet: A vision for the road ahead," *Science* **362**(6412), eaam9288 (2018).

[4] Huggins, W., O'Gorman, B., and Rubin, N. e. a., "Unbiasing fermionic quantum monte carlo with a quantum computer.," *Nature* **603**, 416–420 (2022).

[5] Biamonte, J., W. P. P. N. e. a., "Quantum machine learning," *Nature* **549**, 195–202 (2017).

[6] Boschi, D., "Experimental realization of teleporting an unknown pure quantum state via dual classical and einstein–podolsky–rosen channels," *Physical Review Letters* **80**.

[7] Giovannetti, V., Lloyd, S., and Maccone, L., "Quantum-enhanced measurements: beating the standard quantum limit.," *Science* **306**, 1330–1336 (2004).

[8] Scarani, V., Bechmann-Pasquinucci, H., Cerf, N. J., Dušek, M., Lütkenhaus, N., and Peev, M., "The security of practical quantum key distribution," *Rev. Mod. Phys.* **81**, 1301–1350 (Sep 2009).

[9] Wootters, W. and Zurek, W., "A single quantum cannot be cloned.," *Nature* **299**, 802–803 (1982).

[10] Ruihong, Q. and Ying, M., "Research progress of quantum repeaters," **1237**, 052032 (2019).

[11] Yin, J., Ren, J., Lu, H., and et al., "Quantum teleportation and entanglement distribution over 100-kilometre free-space channels.," *Nature* **488**, 185–188 (2012).

[12] Honjo, T., Nam, S., Takesue, H., Zhang, Q., Kamada, H., Nishida, Y., Tadanaga, O., Asobe, M., Baek, B., Hadfield, R., Miki, S., Fujiwara, M., Sasaki, M., Wang, Z., Inoue, K., and Yamamoto, Y., "Long-distance entanglement-based quantum key distribution over optical fiber.," *Opt. Express* **16**, 19118–19126 (2008).

[13] Yin., J., Cao., Y., Li., Y.-H., and et .al., "Satellite-based entanglement distribution over 1200 kilometers," *Science* **356**(6343), 1140–1144 (2017).

[14] Bell, J. S., "On the einstein podolsky rosen paradox," *Physics Physique* **1**, 195–200 (1965).

[15] Sun, Q.-C., Jiang, Y.-F., Mao, Y.-L., and et. al., "Entanglement swapping over 100 km optical fiber with independent entangled photon-pair sources," *Optica* **4**, 1214–1218 (Oct 2017).

[16] Lu, C., Yang, T., and Pan, J., "Experimental multiparticle entanglement swapping for quantum networking.," *Phys Rev Lett.* **103** (2009).

[17] Goebel, A., Wagenknecht, C., Zhang, Q., Chen, Y., Chen, K., Schmiedmayer, J., and Pan, J., "Multistage entanglement swapping.," *Phys Rev Lett.* **101** (2008).

[18] Bromberg, Y., Lahini, Y., Small, E., and et al., "Hanbury brown and twiss interferometry with interacting photons.," *Nature Photonics* **4**, 721–726 (2010).